Journal of Marine Research, 41, 769–792, 1983

Upwelling rates for the equatorial Pacific Ocean derived from the bomb ^{14}C distribution

by P. D. Quay[1], M. Stuiver[2] and W. S. Broecker[3]

ABSTRACT

A north-south cross section of bomb-produced radiocarbon (^{14}C) in the upper 1000 m of the central equatorial Pacific Ocean (CEP) was measured in April, 1979 during Leg 3 of the NORPAX shuttle experiment. The ^{14}C shows an equatorial mixed layer depletion of ~40‰ compared to subtropical surface waters. Upwelling of deeper, ^{14}C depleted water maintains this minimum. Two subsurface tongues of high ^{14}C water, found north and south of the equator, are associated with high salinity water and probably result from exchange with subtropical surface water. The continued increase in mixed layer ^{14}C levels in the CEP (up to 1979) indicates the importance of ^{14}C input from these subsurface ^{14}C maxima. Equatorward meridional advection resulting from geostrophic flow is the predominant supply of water upwelling at the equator and controls the ^{14}C distribution in the CEP. The results of multi-layer mixing model calculations indicate an upwelling transport rate of 47 Sverdrups (5S–4N) and a maximum depth of upwelling of 225 m (σ_0 = 26.5). These equatorial circulation characteristics explain the ^{14}C, ΣCO_2, oxygen, salinity and tritium distributions measured during Leg 3. The time history of mixed layer bomb ^{14}C concentrations in the CEP indicate an exchange time of 4–6 years between the subtropical and equatorial surface oceans.

1. Introduction

The oceanographic evidence for equatorial upwelling has long been observed (e.g., Sverdrup *et al.*, 1942). Determinations of the rates of equatorial upwelling and the portion of the water column from which this upwelling water is derived have been more difficult. Recently, Wyrtki (1981) has estimated upwelling rates in the equatorial Pacific Ocean by examining mass, heat and salt balances. Equatorial upwelling rates have been determined for the Atlantic Ocean from chemical and isotopic mass balances (Broecker *et al.*, 1978). Halpern (1980) calculated upwelling rates at the equator in the eastern Pacific using horizontal flow measurements. Direct measurements of upward advection rates in the CEP have not been made.

1. Department of Geological Sciences and School of Oceanography, University of Washington, Seattle, Washington, 98195, U.S.A.

2. Department of Geological Sciences and Quaternary Research Center, University of Washington, Seattle, Washington, 98195, U.S.A.

3. Lamont-Doherty Geological Observatory, Palisades, New York, 10964, U.S.A. and Department of Geological Sciences, Columbia University, New York, New York, 10027, U.S.A.

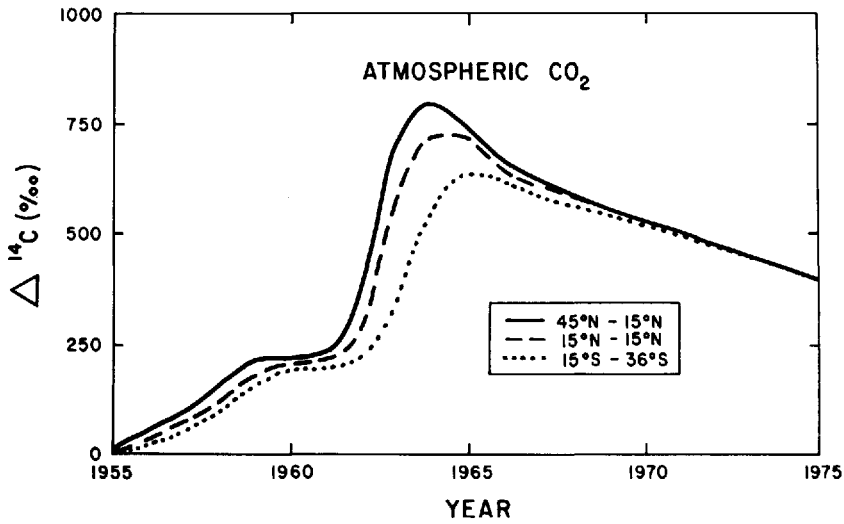

Figure 1. The measured time history of the atmospheric bomb ^{14}C levels (Nydal *et al.*, 1980).

In the following discussion, the results of detailed radiocarbon (^{14}C) measurements made during Leg 3 (April 1979) of the NORPAX Shuttle experiment in the equatorial Pacific will be presented. The present ^{14}C activities in the upper ocean (<1,000 m) are derived from oceanic exchange with atmospheric CO_2 which has been raised to high ^{14}C levels as a result of nuclear bomb testing (Fig. 1). Estimates of the rate of equatorial upwelling and the source of this water will be made based on the measured bomb ^{14}C distributions. We develop a mixing model which describes the distribution of ^{14}C, dissolved inorganic carbon (ΣCO_2), oxygen (O_2), salinity and tritium in the upper portion of the central equatorial Pacific Ocean.

2. Measurements

The cruise track and sampling locations for Leg 3 are shown in Figure 2. The water samples for ^{14}C determinations were collected using 250-l Gerard barrels. The CO_2 was extracted and then collected in NaOH using a modification of the method used by Fonselius and Ostlünd (1959).

The procedure used for determining ^{14}C activity at the Quaternary Isotope Laboratory at the University of Washington has been described previously (Stuiver and Robinson, 1974). The activity of ^{14}C is reported as the ratio $^{14}C/^{12}C$ using the $\Delta^{14}C$ scale in per mill (‰) units (Stuiver and Polach, 1977). The average precision of the $\Delta^{14}C$ determination for a seawater sample is ±4‰. Approximately 400 seawater samples were collected for ^{14}C activity measurement during the shuttle experiment. Meridional profiles (17S–20N) of mixed layer ^{14}C activities were measured on Legs 3, 5, 7, 9, 11, 13 and 15. A meridional cross section of the ^{14}C depth distribution

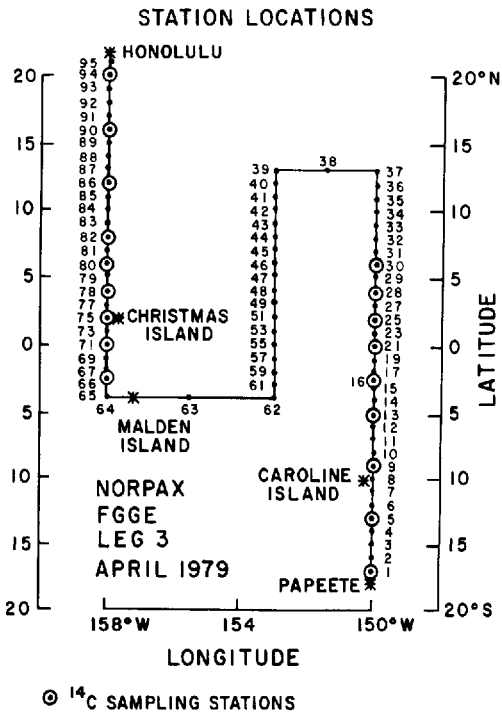

Figure 2. The cruise track and sampling locations for Leg 3 of the NORPAX FGGE shuttle (April 1979).

(<1000 m) was measured during Leg 3. Only the data measured during Leg 3 will be presented here.

Continuous depth profiles of temperature and salinity were measured by the Scripps' Physical and Chemical Oceanographic Data Facility (PCODF) group using a Neil Brown CTD. Discrete measurements of oxygen, nutrients and ΣCO_2 were carried out by PCODF using analytical methods utilized during the GEOSECS program with similar precision in the analyses. The partial pressure of CO_2 gas in water samples (pCO_2)was measured using the method developed by Takahashi (1961) with a precision of ±1.5%. A complete description of the nutrient measurements made during Leg 3 of the NORPAX shuttle experiment is found in Broecker *et al.* (1983).

3. Results

A meridional cross section of mixed layer $\Delta^{14}C$ values is shown in Figure 3. The equatorial mixed layer $\Delta^{14}C$ is ~40‰ more deplete than the subtropical regions. The minimum $\Delta^{14}C$ levels are located between 5S–5N with a mean value of 97 ± 2‰. The northern subtropical surface waters have significantly higher $\Delta^{14}C$ levels (~20‰) than the southern subtropical surface waters. This asymmetry has been maintained even

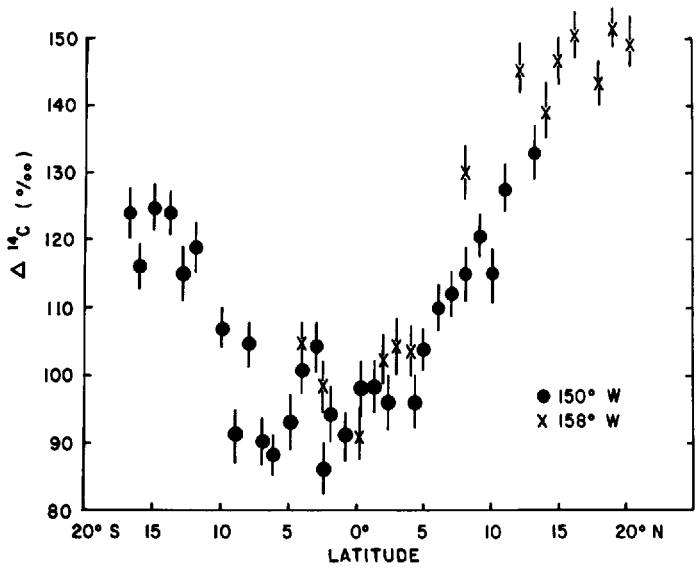

Figure 3. A meridional cross-section of the surface mixed layer $\Delta^{14}C$ concentrations.

though the northern and southern atmospheric ^{14}C levels (Fig. 1) have been similar for the past 10 years (prior to NORPAX), the ^{14}C isotopic equilibration time of the mixed layer ΣCO_2 (i.e., Broecker *et al.*, 1980).

Measured mixed layer nutrient distributions (e.g., ΣCO_2, NO_3, PO_4) show equatorial maxima (Fig. 4), as discussed by Broecker *et al.* (1983). Both the ^{14}C and nutrient mixed layer distributions would result from the upwelling of deeper, ^{14}C depleted and nutrient enriched water.

A meridional cross section of the ^{14}C depth distribution is presented in Figure 5a. Two subsurface tongues of high ^{14}C water are evident north and south of the equator and correspond to the locations of high salinity water, shown in Figure 5b. Similar correlations between tritium and salinity in subsurface waters located at 10N–20N have been observed (Michel and Suess, 1975; Fine *et al.*, 1981). Reid (1973) states that the subsurface equatorial salinity maximum is derived from isopycnal exchange with subtropical surface water. The cross section of $\Delta^{14}C$ vs. density (σ_0) presented in Figure 6 indicates that the subsurface ^{14}C maxima are found at σ_0 = 24.5–25 in the northern hemisphere and at σ_0 = 25–25.5 in the southern hemisphere. Winter surface waters of this density are located between 25N–30N and 27S–35S, respectively (Reid, 1969). The Pacific GEOSECS ^{14}C measurements of surface waters at 25N–30N were 170–195‰, whereas at 27S–35S ^{14}C values were 140–170‰ (Ostlünd and Stuiver, 1980). These surface water ^{14}C levels, although measured in 1974, correspond closely to the maximum ^{14}C values measured during NORPAX. Thus the salinity, density and ^{14}C characteristics of the shallow (100–150 m), subsurface water masses at the poleward boundary of the equatorial ocean indicate that some of the chemical properties of the equatorial ocean are derived from subtropical surface waters.

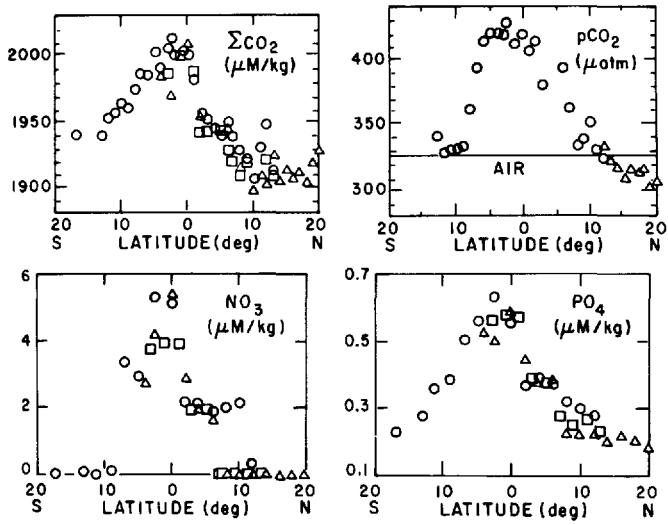

Figure 4. Meridional cross-sections of surface mixed layer concentrations of ΣCO_2, pCO_2, NO_3 and PO_4 (0, 150W; □, 153W; Δ, 158W; from Broecker *et al.*, 1983).

The large north-south ^{14}C gradients are restricted to waters with densities of $\sigma_0 < 26.5$. Waters of these densities outcrop at the surface in both the northern and southern oceans (Reid, 1969), indicating that atmosphere-ocean exchange and subsequent isopycnal transport influence the ^{14}C depth distribution in the equatorial Pacific Ocean. Waters denser than $\sigma_0 = 26.5$ have no measurable north-south ^{14}C gradients along isopycnal surfaces, suggesting that heterogeneous ^{14}C input to isopycnal surfaces where $\sigma_0 > 26.5$ is small relative to the rate of isopycnal mixing.

The ^{14}C vs. σ_0 distribution indicates that the surface depletion of ^{14}C levels near the equator (5S–5N) extends downward to waters where $\sigma_0 \leq 26$. This water mass is bounded to the north and south by waters with high ^{14}C levels and by the atmosphere with higher ^{14}C levels (i.e., 330‰ in 1979; Nydal *et al.*, 1980). Upwelling of deeper ($\sigma_0 > 26$), ^{14}C depleted water into the equatorial ocean is a likely mechanism to maintain a surface water ^{14}C depletion, as discussed below.

A time history of equatorial Pacific mixed layer bomb ^{14}C levels is presented in Figure 7. The mixed layer ^{14}C values for the eastern equatorial Pacific (EEP) are derived from ^{14}C measurements on corals collected from the Galapagos Is. (Druffel, 1980), whereas direct surface ^{14}C measurements between 125W–170E were obtained for the central equatorial Pacific (CEP). The ^{14}C time history of these two portions of the equatorial Pacific differ remarkably. The EEP mixed layer ^{14}C levels reach a constant value in 1970, whereas in the CEP the ^{14}C levels continue to increase until 1979, while atmospheric ^{14}C levels have been decreasing (Fig. 1). This continued increase in ^{14}C levels in the CEP results from equatorward, meridional transport of ^{14}C from the subsurface tongues of high ^{14}C water, as discussed below.

Individual $\Delta^{14}C$ vs. σ_0 profiles are plotted in Figure 8a. Near the equator the $\Delta^{14}C$

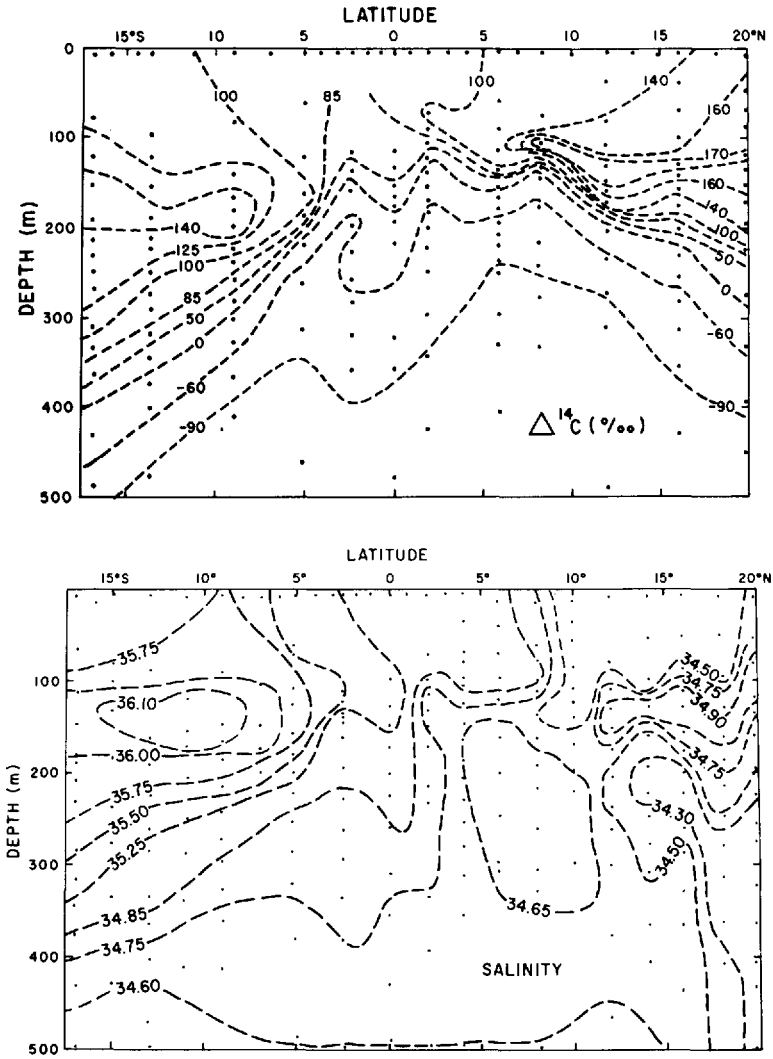

Figure 5. (a) A meridional cross-section of the depth distribution of $\Delta^{14}C$. (b) A meridional cross-section of the depth distribution of salinity.

levels are nearly constant down to $\sigma_0 \simeq 25.5$ and decrease sharply below. The ^{14}C profiles measured between 9S–5S and 6N–8N have a subsurface maximum at σ_0 = 24.5–25.5, corresponding to the tongues of high ^{14}C water located north of 8N and south of 9S. Profiles of $\Sigma^{14}CO_2$ (i.e., $^{14}C/^{12}C$ * ΣCO_2) are shown in Figure 8b. All profiles show a subsurface maximum in $\Sigma^{14}CO_2$ at σ_0 = 25–26. The surface layers between 9S–8N show little change in $\Sigma^{14}CO_2$, indicating the poleward increase in $\Delta^{14}C$ (Fig. 3) is approximately balanced by the poleward decrease in ΣCO_2 (Fig. 4).

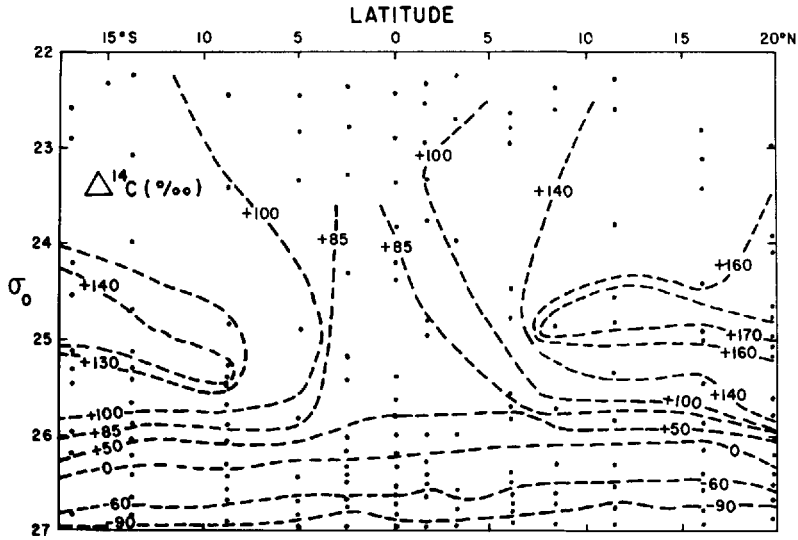

Figure 6. A meridional cross-section of $\Delta^{14}C$ vs. σ_0.

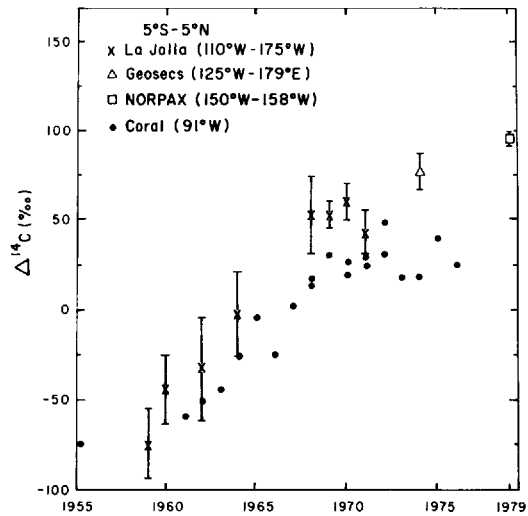

Figure 7. The time history of equatorial mixed layer ^{14}C levels. Surface ^{14}C measurements include those made at La Jolla (Linick, 1978), during GEOSECS (Ostlünd and Stuiver, 1980), during Leg 3 of the FGGE shuttle and on corals collected on one of the Galapagos Is. (Druffel, 1980).

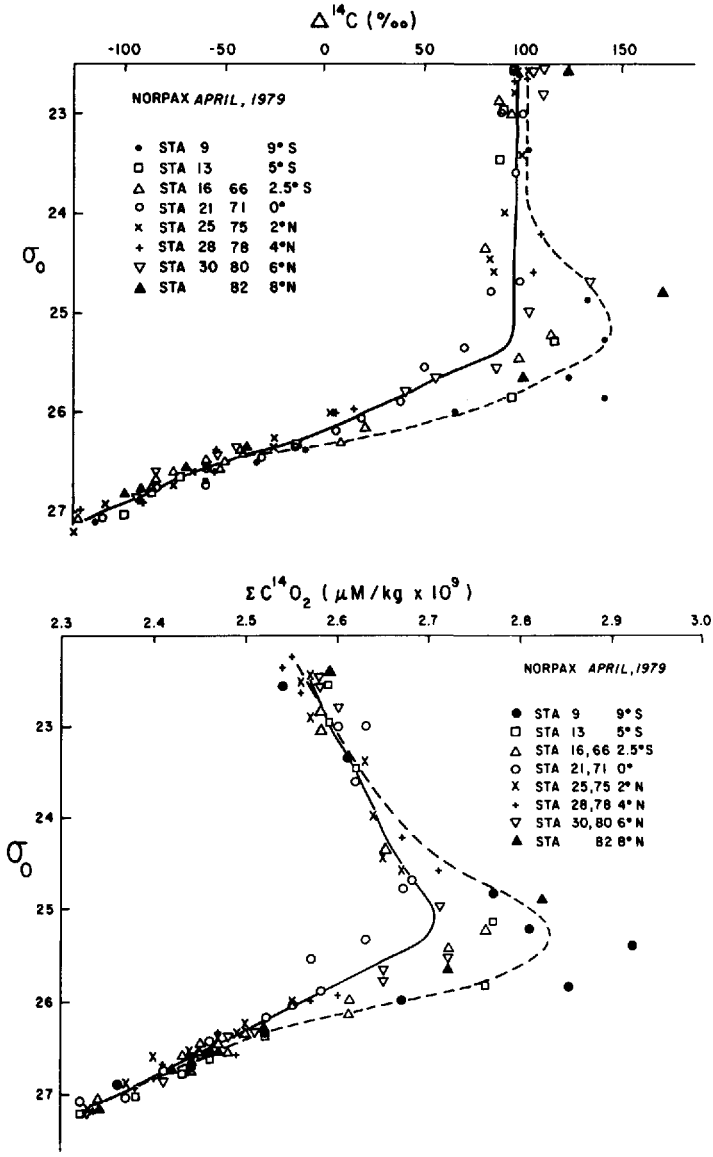

Figure 8. (a) $\Delta^{14}C$ vs. σ_0 profiles for stations located between 9S–8N. (b) $\Sigma^{14}CO_2$ vs. σ_0 profiles for stations located between 9S–8N.

4. Discussion

Several characteristics of the ^{14}C distribution measured during the NORPAX shuttle experiment provide insight into understanding the important processes which determine the chemistry of the equatorial Pacific Ocean. First, the ^{14}C-depleted and nutrient-enriched surface layer indicate the input of deeper water. Second, the two

subsurface ^{14}C maxima located at 100–150 m toward the poleward boundaries of the equatorial ocean are sources of ^{14}C which result from isopycnal mixing with subtropical surface waters. Third, the difference in mixed layer ^{14}C time histories in the CEP and EEP reflect the importance of meridional ^{14}C transport. In the following discussion, we will address three questions: Is "local" upwelling (derived from subsurface, equatorward meridional advection) or upwelling at the eastern boundary and subsequent westward transport the most important upwelling mechanism influencing equatorial ocean chemistry? What is the rate of equatorial upwelling? From what depths is the upwelling water derived?

The equatorial surface oceans are dominated by zonal current systems. East-west current velocities are high. Profiling current meter measurements made during the NORPAX Shuttle experiment (Wyrtki *et al.*, 1980) result in maximum speeds of 60 cm s^{-1} for the North Equatorial Current (NEC), 80 cm s^{-1} for the South Equatorial Current (SEC), 125 cm s^{-1} for Equatorial Undercurrent (EUC) and 50 cm s^{-1} for the North Equatorial Countercurrent (NECC). The meridional component of equatorial velocities is much smaller and thus more difficult to directly measure. The results of models used to study wind-driven equatorial circulation imply the existence of equatorward meridional velocities (<10 cm s^{-1}) associated with the strong zonal flow of the EUC below the base of the mixed layer (e.g., McCreary, 1981).

Wyrtki (1981) measured east-west pressure gradients and calculated geostrophic flow near the equator; he also estimated surface Ekman divergence from meteorological data. Although the meridional velocities are small (i.e., <5 cm s^{-1}), the water transport is large when integrated over the east-west extent of the equatorial ocean. Thus Wyrtki (1981) estimates a total equatorward, geostrophic transport of 70–84 Sv (between 170E and 100W), of which 33–38 Sv is in the surface mixed layer. His estimate of total Ekman divergence at 5N and 5S (between 170E–100W) is 84 Sv, thus 70–100% of the upwelling water balancing Ekman divergence can be derived from geostrophic convergence. These water transports are large compared to zonal transports near the equator (i.e., 3S–3N). For example, Wyrtki *et al.* (1980) estimate transports of 20 Sv for the SEC and 40 Sv for the EUC.

Assuming the majority of the water upwelling into the equatorial mixed layer is supplied by local geostrophic flow, then the chemical (and tracer) characteristics of the equatorial Pacific Ocean will be strongly influenced by chemical properties of the water masses located at the poleward boundaries of the equatorial ocean. Thus east-west chemical gradients near the equator likely reflect the east-west gradients at the northern and southern boundaries of the equatorial ocean. However, strong zonal recirculation and atmosphere-ocean interaction should reduce the equatorial east-west gradients relative to those present at the poleward boundaries.

The time histories of bomb ^{14}C in the mixed layers of the eastern and central equatorial ocean (Fig. 7) are evidence for the importance of local upwelling processes. The continued increase in CEP ^{14}C levels after 1970 while ^{14}C levels in EEP were constant cannot be the result of westward transport of surface water, but must be the

result of geostrophic transport of ^{14}C from the subsurface ^{14}C maxima located toward the poleward boundaries of the equatorial Pacific Ocean. Furthermore, the increase in equatorial mixed layer ^{14}C levels until 1979 implies that the ^{14}C levels of the subsurface ^{14}C maxima have increased between 1965–1979. This observation suggests that these subsurface water masses have ^{14}C levels which represent the ^{14}C concentrations of subtropical surface water during earlier times of higher atmosphere and ocean mixed layer ^{14}C levels, as discussed below.

The physical oceanographic data and bomb ^{14}C measurements in the equatorial Pacific Ocean indicate that geostrophic transport is the predominant process supplying water for equatorial upwelling. In the following discussions, we will use the measured bomb ^{14}C and chemical distributions to determine the rate of upwelling and the depths from which the upwelling water is derived. Because of the predominance of meridional transport, we will utilize a two-dimensional (north-south and depth) mixing model to examine equatorial upwelling, assuming that the net east-west transport of dissolved chemicals is negligible compared to north-south transport for the CEP.

The equatorial ocean is divided into three latitude bands 9S–5S, 5S–4N and 4N–8N. The central latitude band encompasses the most depleted ^{14}C mixed layers (Fig. 3). Its poleward boundaries (specified by the station locations) closely correspond to those chosen by Wyrtki (1981) to calculate Ekman and geostrophic transports. The two poleward latitude bands represent the next adjacent interval that can be adequately described by the ^{14}C sampling intervals. The poleward boundary of these intervals borders on the equatorward edge of the subsurface ^{14}C maxima (Fig. 5a). The chemical properties of these three sections were estimated using data collected at stations located at 9S, 5S, 2.5S, 0°, 2N, 4N, 6N and 8N.

To determine the depths (density levels) which supply the water upwelling into the mixed layer, the upper equatorial ocean is divided into 15 layers: a 50 m deep mixed layer, eight 25 m deep layers, three 50 m deep layers and three 100 m deep layers down to 700 m ($\sigma_0 = 27.25$). A schematic representation of the model is presented in Figure 9.

Meridional transport is parameterized in terms of isopycnal advection (V) and diffusion (K_y). The concentrations of $\Delta^{14}C$, ΣCO_2, NO_3 and O_2 for each layer in the poleward boundaries (5S–9S and 4N–8N) are fixed equal to the average measured values. Initially, it is assumed the advection and diffusion rates are equal across the northern and southern boundaries (i.e., 5S and 4N).

Vertical exchange within the central latitude band is parameterized as vertical advection (W) and diffusion (K_z). To conserve mass, the depth integrated meridional equatorward transport below the mixed layer (plus any upwelling originating within the 5S–4N region) is balanced by the poleward divergence of water within the mixed layer. Concentrations in the bottom layer (z = 600–700 m, σ_0 = 27.15–27.25) are fixed as the bottom boundary condition.

The equatorial distribution of ^{14}C, ΣCO_2 and O_2 are also dependent on gas exchange

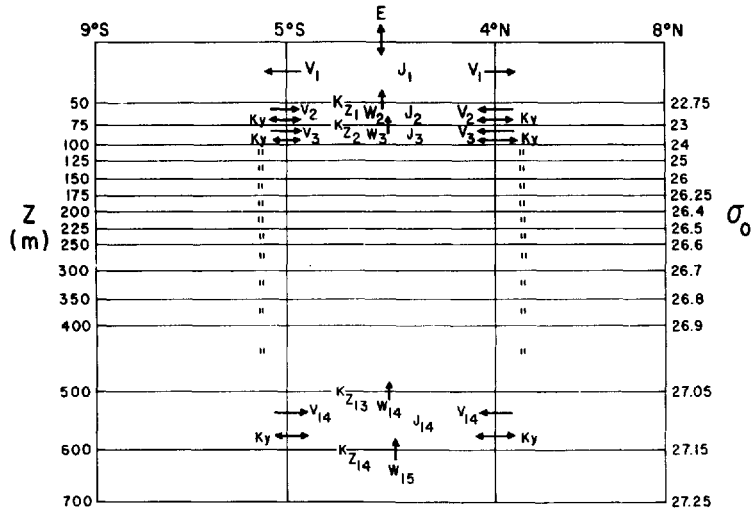

Figure 9. A schematic representation of the mixing model used to calculate ^{14}C, ΣCO_2, O_2, salinity and tritium profiles for the 5S–4N equatorial region. The concentration in the poleward boundaries (5S–9S and 4N–8N) and bottom layer (600–700 m) are fixed. A description of the model parameters is presented in Table 1.

with the atmosphere. The rate of gas exchange (E) is parameterized as a "piston velocity" describing the rate of flushing of dissolved gases through the water column (Broecker and Peng, 1974). Also the time rate of change of nutrients (and ^{14}C) depends on the rate of biological uptake and release (J). Values for J are calculated for each layer in the model using a NO_3 balance calculated from the measured NO_3 concentrations.

The equations describing the time rate of change of NO_3, ΣCO_2, $\Delta^{14}C$ and O_2 for each layer are presented in Table 1.

Steady state solutions are calculated for ^{14}C, ΣCO_2 and O_2. Although the bomb ^{14}C in the upper ocean is a transient phenomenon, its distribution in the equatorial ocean can be in a "quasi" steady state. This occurs if the water replacement time is short enough so that the source of ^{14}C (i.e., atmosphere, poleward boundaries) changes little over the residence time of the water. We will show that this situation occurs in the central equatorial Pacific. A near steady state for ^{14}C is suggested by the slight increase in mixed layer $\Delta^{14}C$ levels measured over the five year interval between GEOSECS (1974) and the NORPAX shuttle (1979), as seen in Figure 7. In addition, we compared the ^{14}C depth profiles calculated (for 1979) using a time-dependent version of the mixing model with those calculated from the steady state version and found the average agreement was ±4‰, approximately equal to the precision of the $\Delta^{14}C$ measurement. To simplify the calculations, steady state ^{14}C distributions were calculated and these results are referred to in the following discussion.

Table 1. The equations describing the time rate of change of NO_3, ΣCO_2, $\Sigma^{14}CO_2$, and O_2 for the model calculations described in the text.

1. $$\frac{d(NO_3)_i}{dt} = \left[V_i\alpha_{bi} + W_{i+1}\alpha_{i+1} - (W_{i+1} + V_i)\alpha_i + \frac{K_y}{\Delta y}(\alpha_{bi} - \alpha_i) + \frac{K_{z_i}}{\Delta Z_{i+1}}(\alpha_{i+1} - \alpha_i) - \frac{K_{z_{i-1}}}{\Delta Z_i}(\alpha_i - \alpha_{i-1}) + J_i^n \right] \cdot \frac{1}{\Delta Z_i}$$

2. $$\frac{d(\Sigma CO_2)_i}{dt} = \left[V_i\beta_{bi} + W_{i+1}\beta_{i+1} - (W_{i+1} + V_i)\beta_i + \frac{K_y}{\Delta y}(\beta_{bi} - \beta_i) + \frac{K_{z_i}}{\Delta Z_{i+1}}(\beta_{i+1} - \beta_i) - \frac{K_{z_{i-1}}}{\Delta Z_i}(\beta_i - \beta_{i-1}) + J_i^n\left(\frac{C}{N}\right)_{org} + E(\beta_a - \beta_m)^* \right] \cdot \frac{1}{\Delta Z_i}$$

3. $$\frac{d(\Sigma^{14}CO_2)_i}{dt} = \left[V_i[\beta_{bi}\gamma_{bi}] + W_{i+1}[\beta_{i+1}\gamma_{i+1}] - (W_{i+1} + V_i)[\beta_i\gamma_i] + \frac{K_y}{\Delta y}[\beta_{bi}\gamma_{bi} - \beta_i\gamma_i] + \frac{K_{z_i}}{\Delta Z_{i+1}}[\beta_{i+1}\gamma_{i+1} - \beta_i\gamma_i] - \frac{K_{z_{i-1}}}{\Delta Z_i}[\beta_i\gamma_i - \beta_{i-1}\gamma_{i-1}] + J_i^n\left(\frac{C}{N}\right)_{org}\gamma_m + E[\beta_a\gamma_a - \beta_m\gamma_m]^* \right] \cdot \frac{1}{\Delta Z_i}$$

4. $$\frac{d(O_2)_i}{dt} = \left[V_i\delta_{bi} + W_{i+1}\delta_{i+1} - (W_{i+1} + V_i)\delta_i + \frac{K_y}{\Delta y}(\delta_{bi} - \delta_i) + \frac{K_{z_i}}{\Delta Z_{i+1}}(\delta_{i+1} - \delta_i) - \frac{K_{z_{i-1}}}{\Delta Z_i}(\delta_i - \delta_{i-1}) - 1.4\,J_i^n\left(\frac{C}{N}\right)_{org} + E(\delta_a - \delta_m)^* \right] \cdot \frac{1}{\Delta z_i}$$

Where

α	is the concentration of NO_3 (moles m^{-3})
β	is the concentration of ΣCO_2 (moles m^{-3})
γ	is the ratio $^{14}C/^{12}C$ of the ΣCO_2
δ	is the concentration of O_2 (moles m^{-3})
*	These terms are only included in mixed layer balance
i	refers to a given depth interval in the multi-layer model (see Fig. 9)
bi	refers to the poleward boundary concentration at a given depth interval
$(C/N)_{org}$	is the carbon/nitrogen ratio in organic particulate matter
β_a	the mixed layer concentration of dissolved CO_2 gas in equilibrium with the atmosphere (moles m^{-3})

Table 1. Continued

β_m	is the mixed layer concentration of dissolved CO_2 gas (moles m^{-3})
δ_a	is the mixed layer concentraton of dissolved O_2 gas in equilibrium with the atmosphere (moles m^{-3})
δ_m	is the mixed layer concentration of dissolved O_2 gas (moles m^{-3})
γ_a	is the C^{14}/C^{12} of atmospheric CO_2
γ_m	is the C^{14}/C^{12} of the mixed layer ΣCO_2
V	is meridional advection rate (m s^{-1})
W	is upward advection rate (m s^{-1})
K_y	is eddy diffusion rate along meridional (m^2 s^{-1})
K_z	is vertical (cross-isopycnal) diffusion rate (m^2 s^{-1})
Z	is depth interval of layer (m)
y	is distance between poleward boundary and central equatorial region (m)
J_i^n	is the production rate of NO_3 resulting from particulate matter degradation (moles m^{-2} s^{-1})
E	is gas piston velocity (m s^{-1})

Equatorial distributions of $\Delta^{14}C$, ΣCO_2 and O_2 are used to determine two important aspects of equatorial circulation: the rate of equatorial upwelling and the depths (density levels) from which the upwelling water is derived.

Our approach is to calculate $\Delta^{14}C$, ΣCO_2 and O_2 profiles for the 5S–4N region, for a range in values of the mixing parameters (i.e., W, E, K_y), while allowing the upwelling water to enter the equatorial region over a range of depths (densities). The best estimates of the model variables are determined by optimizing the agreement between calculated and observed profiles.

Because the model calculations require estimates of several mixing parameters, we have reduced the number of variables by making three assumptions. First, we assume that below the mixed layer the equatorward meridional velocity decreases linearly with depth, as indicated by the linear decrease with depth of the dynamic height difference and resulting geostrophic velocities calculated at 5S and 5N (see Fig. 4 in Wyrtki, 1981). Second, we assign values to the vertical (cross-isopycnal) eddy diffusivities based on the microstructure measurements of energy dissipation rates in the equatorial ocean (Osborn, 1980; Crawford and Osborn, 1981). These investigators find the highest energy dissipation in the depth region (<150 m) above the Equatorial Undercurrent (EUC). Within the core of the EUC (150–250 m), the lowest rates are measured. Below the EUC, the dissipation rates rise slightly. Following their estimates of K_z, we assign values of K_z = 1 cm^2s^{-1} between 50–150 m, 0.02 cm^2s^{-1} between 150–250 m and 0.1 cm^2s^{-1} below 250 m. Because the model K_z values represent the 5S–4N region, we use lower values than those measured at the equator (±1°) by Osborn (1980) and Crawford and Osborn (1981). Third, the rate of horizontal (along isopycnal) diffusion (K_y) is assumed to be constant with depth.

Steady state ^{14}C, ΣCO_2 and O_2 profiles were calculated for several values of gas exchange rates, upwelling velocities, horizontal diffusion rates and the maximum

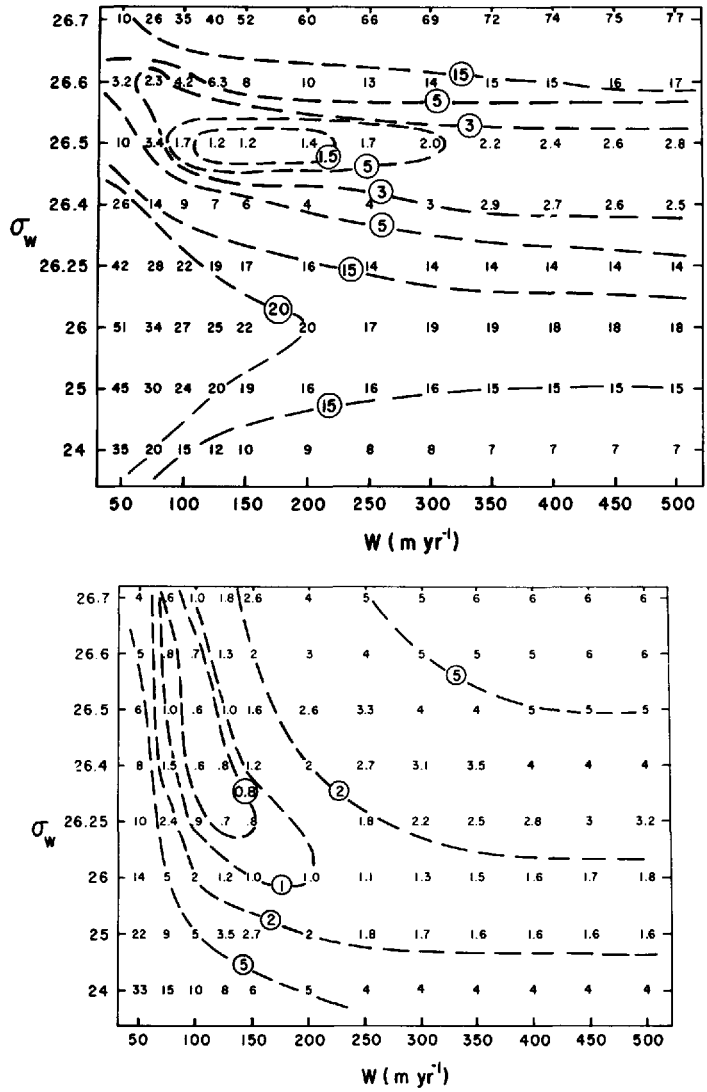

Figure 10. (a) The dependence of the reduced chi square (χ_ν^2) values of the model calculated $\Delta^{14}C$ profiles on W and σ_ω. (b) The dependence of the reduced chi square (χ_ν^2) values of the model calculated ΣCO_2 profiles on W and σ_ω. (c) The dependence of the reduced chi square (χ_ν^2) values of the model calculated O_2 profiles on W and σ_ω.

density with which upwelling water enters the equatorial region (σ_ω). A reduced chi square (χ_ν^2) parameter is used to estimate the goodness of fit of model calculated and measured profiles of $\Delta^{14}C$, ΣCO_2 and O_2. The χ_ν^2 value compares the difference between the measured and model calculated values for each depth (density) layer to the uncertainty of the measured value (i.e., $\chi_\nu^2 = 1/V \cdot \Sigma[1/\sigma_i^2 (Y_i - Y(x_i))^2]$ where Y_i

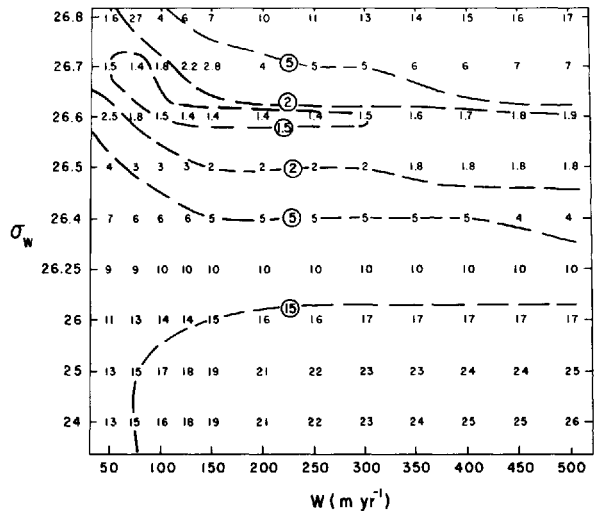

is the measured value, σ_i is the uncertainty in Y_i, $Y(x_i)$ is the estimate of Y_i, and V is the degree of freedom; Bevington, 1969). The model estimates are good approximations to the observed values where $\chi_\nu^2 \leq 1$. The model calculated $\Delta^{14}C$, ΣCO_2 and O_2 profiles are most sensitive to values of W and σ_ω and less sensitive to values of E and K_y, as discussed below. Thus, the sensitivity of the agreement between calculated and observed profiles to W and σ_ω will be initially examined. The χ_ν^2 values for the calculated $\Delta^{14}C$ profiles as a function of W and σ_ω are presented in Figure 10a. For these calculations, $E = 2.8$ m d^{-1} (15 moles CO_2 m^{-2}yr^{-1}) and $K_y = 10^7$ cm^{2}s^{-1}, as discussed below. These results indicate that the calculated ^{14}C profiles are more sensitive to σ_ω than W. The best fit (minimum χ_ν^2) occurs when the meridional advection supplying the upwelling water extends down to $\sigma_0 = 26.5$ (~225 m). However, χ_ν^2 is not strongly dependent on W, for $W \geq 100$ m yr^{-1}. The relative insensitivity of χ_ν^2 to W occurs at larger values of W where upwelling, rather than gas exchange, dominates the supply of ^{14}C to the equatorial ocean. In this situation, the ^{14}C level of the equatorial ocean depends only on the ^{14}C level of the upwelling water, not the rate at which it upwells (W). With fixed boundary concentrations of ^{14}C, the average ^{14}C of the upwelling water is a function of only σ_ω.

The agreement between calculated and measured ΣCO_2 profiles (Fig. 10b) is more sensitive to W than σ_ω. The equatorial ΣCO_2 balance is essentially maintained by the input rate of ΣCO_2 by the upwelling water and the loss of ΣCO_2 out of the mixed layer by Ekman divergence, gas exchange, and particulate loss. The CO_2 loss via gas exchange results from the higher partial pressure of CO_2 gas in the water (~410 μatm) than in the atmosphere (~326 μatm), see Broecker *et al.* (1983). The reduced sensitivity of the calculated ΣCO_2 profiles to σ_ω can be explained by the observation that in the equatorial region for waters with $[NO_3] > 10$ μM (i.e., $\sigma_0 > 25$), the rate of

increase in ΣCO_2 and NO_3 is in approximately the Redfield ratio, as indicated by Broecker *et al.* (1983). Thus, for waters upwelling from depths where $\sigma_0 > 25$, the resulting increase of ΣCO_2 advected into the equatorial ocean is approximately balanced by the additional particulate loss of ΣCO_2 resulting from the increased NO_3 input.

The χ_ν^2 values obtained for the calculated O_2 profiles (Fig. 10c) are more sensitive to σ_ω than W, as observed for the calculated $\Delta^{14}C$ profiles. The χ_ν^2 minimum is calculated for a deeper maximum upwelling depth than for ^{14}C (i.e., $\sigma_\omega = 26.6$) which probably results from the eastward transport of O_2 by the EUC at 150–250 m (Tsuchiya, 1968). Zonal transport is not parameterized by the two-dimensional model discussed here. The ^{14}C and ΣCO_2 depth profiles are less sensitive to the EUC transport because the atmosphere-mixed layer equilibration times for $\Sigma^{14}CO_2$ and ΣCO_2 are respectively 10 years and 1 year, as compared to ~1 month for O_2 (i.e., Broecker *et al.*, 1980). Thus previous atmospheric contact by waters eventually contributing to the EUC will affect the O_2 concentration much more than ^{14}C or ΣCO_2, increasing the east-west O_2 gradients as observed by Tsuchiya (1968).

As mentioned, values of $\chi_\nu^2 \leq 1$ indicate which values of W and σ_ω result in reasonable fits to the data. For the calculated ΣCO_2 profiles this criterion is met where $W = 75-150$ m yr^{-1} (Fig. 10b). The fit to the ^{14}C data is less good, a minimum $\chi_\nu^2 = 1.2$ where $W = 125-150$ m yr^{-1} and $\sigma_\omega = 26.5$. For the O_2 profiles a minimum χ_ν^2 value of 1.4 is calculated for $W = 125 - 250$ m yr^{-1} and $\sigma_\omega = 26.6$.

The χ_ν^2 values of calculated ^{14}C, ΣCO_2 and O_2 profiles are not very sensitive to gas exchange rates or horizontal diffusion rates where $E < 3.4$ m d^{-1} and $K_y \leq 10^7$cm^{2}s^{-1}, as seen in Figure 11. The optimum χ_ν^2 values were obtained where $E = 2.8 \pm 0.6$ m d^{-1} (15 ± 3 moles CO_2 m^{-2} yr^{-1}) and $K_y = 10^7$ cm^{2}s^{-1}. These gas exchange rates compare to ocean wide averages of 2.9 ± 0.7 m d^{-1} (16 ± 4 moles CO_2 m^{-2} yr^{-1}) calculated from radon and pre-bomb ^{14}C measurements (Peng *et al.*, 1979; Stuiver, 1980). Previous estimates of subsurface horizontal diffusion rates vary from 10^3-10^7 cm^2 s^{-1} for length scales <500 km (Kullenberg, 1974).

In summary, the best estimates of the model parameters describing equatorial upwelling are: $W = 110 \pm 30$ m yr^{-1}, $\sigma_\omega = 26.5$, $E = 2.8 \pm 0.6$ m d^{-1} and $K_y \leq 10^7$ cm^{2}s^{-1}. The steady state profiles of $\Delta^{14}C$, ΣCO_2 and O_2 calculated for the above values of model parameters are compared to the measured profiles in Figure 12.

An upwelling rate of 110 ± 30 m yr^{-1} corresponds to an average equatorward velocity of 1.0 ± 0.3 cm s^{-1} over the 50–225 m depth interval and results in 47 ± 13 Sv upwelling through the base of the mixed layer for an equatorial region bounded by 150E–90W and 5S–4N. For an equatorial region bounded by 170E–100W and 5S–5N as described by Wyrtki (1981), an upward transport rate of 39 ± 11 Sv is calculated for $W = 110 \pm 30$ m yr^{-1}. This transport estimate is within the range (37 Sv–51 Sv) determined by Wyrtki (1981), based on water balance calculations. An upwelling rate of 110 ± 30 m yr^{-1} into the equatorial mixed layer corresponds to a meridionally

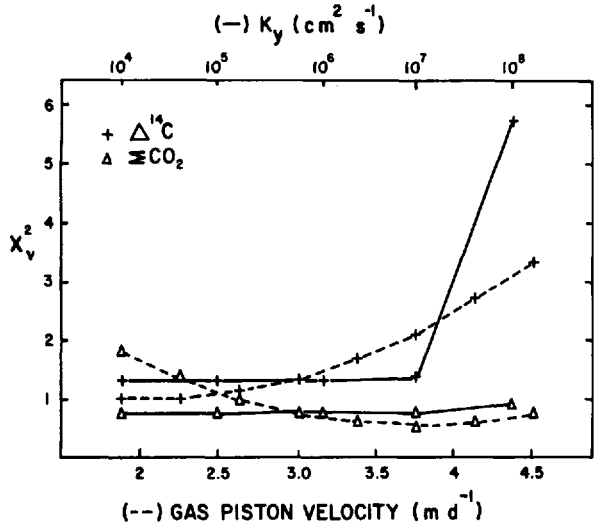

Figure 11. The dependence of the reduced chi square (χ_v^2) values of the model calculated $\Delta^{14}C$ and ΣCO_2 profiles on the horizontal diffusion rate (K_y) and the gas piston velocity (E).

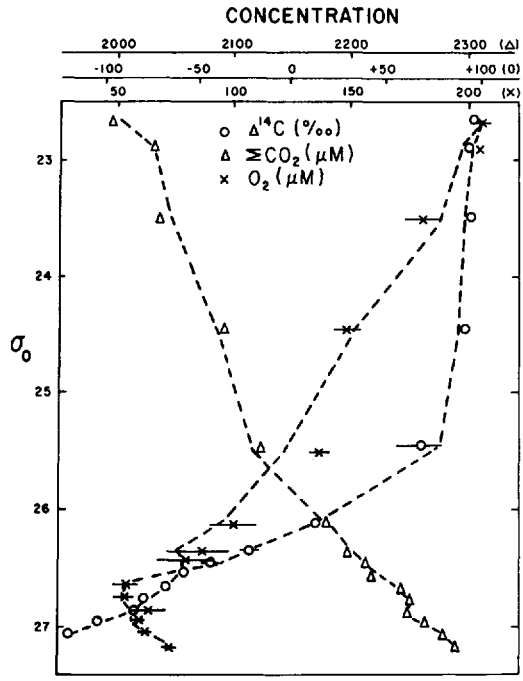

Figure 12. A comparison of the model calculated $\Delta^{14}C$, ΣCO_2 and O_2 profiles (---) with the average concentrations measured between 5S–4N. W = 110 m yr^{-1}; σ_ω = 26.5.

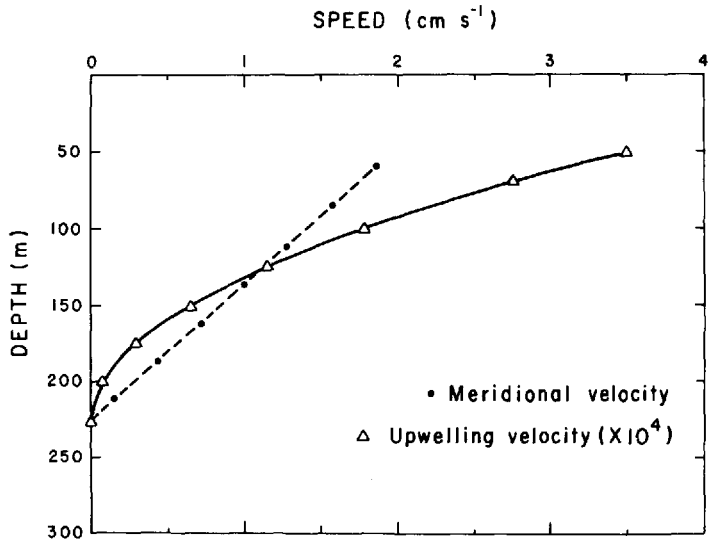

Figure 13. A depth profile of the model calculated meridional velocity and upwelling velocity where the upwelling rate at the base of the mixed layer is 110 m yr^{-1} and $\sigma_\omega = 26.5$.

integrated (5S–5N) transport of 3.9 ± 1.1 m^2s^{-1}. In comparison, Wyrtki (1981) estimates the Ekman divergence in the CEP to be 4.0 m^2s^{-1} at 5N and 4.4 m^2s^{-1} at 5S. The equatorial mixed layer water balance must also include equatorward geostrophic transport, which Wyrtki (1981) estimates at 1.9 m^2s^{-1} at 5N and 5S (using pressure gradients measured at 3N and 3S). Thus, within the uncertainty of our model calculated upwelling rate, a mixed layer water balance is maintained by water entering via upwelling and geostrophic flow and leaving via Ekman divergence. Also our estimate of 225 m as the maximum depth of upwelling coincides with Wyrtki's (1981) estimate of the maximum depth of geostrophic convergence (see Fig. 4, Wyrtki, 1981). Calculated depth profiles of W and V for $W = 110$ m yr^{-1} and $\sigma_\omega = 26.5$ are presented in Figure 13.

As a further test of the model results, we examined the equatorial distributions of tritium and salinity. Like ^{14}C, tritium is a bomb-produced radionuclide. However, its distribution in the oceans is distinctly asymmetric with the large majority located in the northern oceans (Fine *et al.*, 1981). This asymmetry shows up dramatically at the equator, as measured during the NORPAX Shuttle experiment (Fine *et al.*, 1983). Thus the tritium distribution in the equatorial Pacific Ocean depends on the relative amounts of water reaching the equator from northern and southern ocean origins. Salinity also shows strong north-south gradients across the equatorial Pacific Ocean, reflecting the input of subtropical and subarctic water (see Fig. 5b).

We calculated the equatorial depth (density) distributions of tritium and salinity using the mixing model described above, for $W = 110$ m yr^{-1} and $\sigma_\omega = 26.5$. Steady

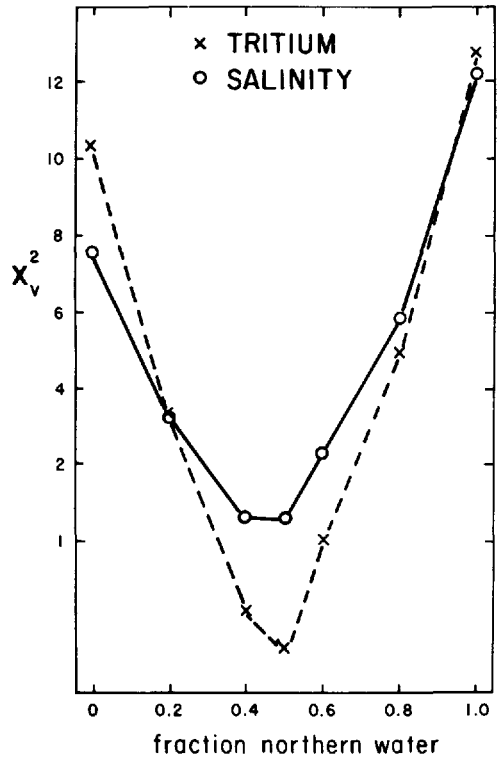

Figure 14. The dependence of χ_ν^2 for the model calculated tritium and salinity profiles on the fraction of water advecting equatorward from the northern boundary. $W = 110$ m yr^{-1}; $\sigma_\omega = 26.5$.

state calculations of average tritium and salinity distributions within the 5S–4N interval were made for variable proportions of water advecting across the northern and southern boundaries. A steady state calculation for tritium is justified if, as for ^{14}C, the time change of tritium is relatively small over the 2 year renewal time of the upper equatorial ocean (i.e., 225 m/110 m yr^{-1}). Although the equatorial tritium distribution has shown some change during the nine year interval between GEOSECS and NORPAX, the major features are similar (Fine *et al.*, 1983). Thus the steady state tritium calculations should indicate whether the model calculated upwelling rates and maximum upwelling depths result in gross miscalculations of the tritium distribution measured during the shuttle experiment.

The sensitivity of the χ_ν^2 values of the calculated tritium and salinity distributions to the fraction of upwelling water advecting across the northern boundary (4N) is presented in Figure 14. These results suggest that an equal transport of water across the northern and southern boundaries produce the best fit to the tritium and salinity data where $W = 110$ m yr^{-1} and $\sigma_\omega = 26.5$. The minimum values of χ_ν^2 for tritium (0.7)

and salinity (1.4) suggest that the model calculated profiles agree well with the data, as shown in Figures 15a and 15b, respectively. Average tritium concentrations for the three latitude bands 8S–4S, 4S–4N and 4N–8N were calculated from tritium measurements made during Legs 3 and 9 of the NORPAX shuttle experiment (Ostlünd, 1981).

The ability of the two-dimensional mixing model to accurately calculate the equatorial distributions of ^{14}C, ΣCO_2, O_2, salinity and tritium implies that meridional geostrophic transport controls the distribution of chemical species in the surface equatorial ocean, as suggested by the mass transport calculations of Wyrtki (1981).

The influence of meridional transport is also apparent in the measured time history of the equatorial Pacific mixed layer ^{14}C levels, see Figure 7. Our results indicate that the equatorial mixed layer water renewal time is <0.5 years (50 m/110 m yr^{-1}) and thus if gas exchange were the major source of ^{14}C to the equatorial ocean, the mixed layer ^{14}C time history would closely follow the atmospheric ^{14}C record. However, the equatorial mixed layer ^{14}C levels continue to increase after the peak in atmospheric ^{14}C levels in 1965; thus there must be an additional source of ^{14}C to the equatorial oceans. The diminished role of atmospheric ^{14}C input is also evident in the negligible difference between the ^{14}C concentration of atmospheric and mixed layer pCO_2 (i.e., $\Delta^{14}C$ * pCO_2) measured during the NORPAX shuttle experiment. There is presently (as of 1979) little net transfer of ^{14}C across the atmosphere-ocean boundary.

The measured lag time between the atmospheric and equatorial mixed layer ^{14}C maxima provides an estimate of the exchange time between subtropical surface water and the equatorial ocean. The increase in equatorial mixed layer ^{14}C levels after 1965 results from mixing with the subsurface tongues of high ^{14}C located at the poleward boundaries of the equatorial ocean. These subsurface water masses have ^{14}C characteristics which were obtained by exchange with surface waters at subtropical latitudes that equilibrated with the atmosphere during earlier times of higher atmospheric ^{14}C levels, as discussed above. The time change in ^{14}C at these subsurface poleward boundaries depends on the exchange time between the equatorial ocean and subtropical surface water. In turn, the ^{14}C time change of the subtropical surface water depends on the time history of the atmospheric ^{14}C levels and the ^{14}C isotopic equilibrium time of the subtropical mixed layer with the atmosphere, which is approximately 10 years (i.e., 100 m * 2 moles CO_2 m^{-3}/20 moles CO_2 m^{-2} yr^{-1}). Thus, by fixing the atmospheric ^{14}C time history and the subtropical mixed layer ^{14}C isotopic equilibration time, we use the equatorial mixing model described above to calculate the equatorial mixed layer ^{14}C time history. The best agreement between model calculated and observed equatorial time histories results when a 4–6 year exchange time exists between the subtropical and equatorial Pacific Ocean (Fig. 16).

For the model calculations, this exchange time is parameterized as the time it takes for water with the ^{14}C concentration of the subtropical mixed layer to "arrive" at the

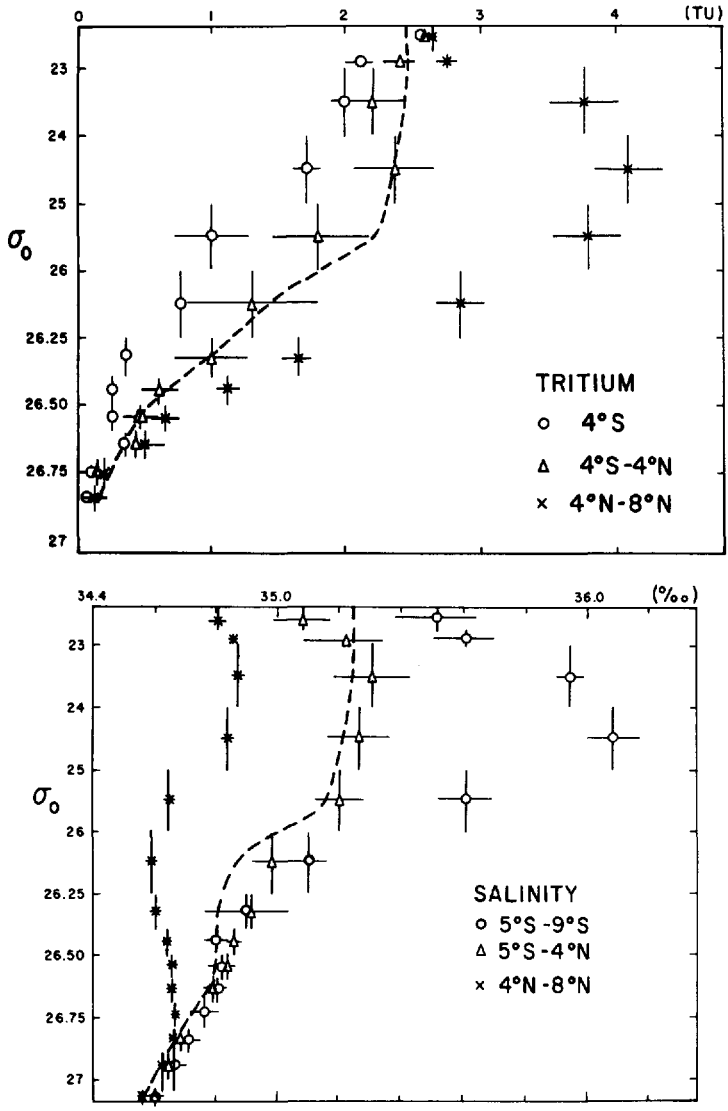

Figure 15. (a) A comparison of the model calculated tritium profile (---) with the average concentrations measured over the 4S–4N interval (Ostlünd, 1981). The average concentrations in the northern poleward boundary 4N–8N and at 4S (the southern extent of the tritium measurements) are also presented. $W = 110$ m yr^{-1}; $\sigma_\omega = 26.5$. (b) A comparison of the model calculated salinity profile (---) with the average concentrations measured over the 5S–4N interval. The average salinities in northern (4N–8N) and southern (5S–9S) boundaries are also presented. $W = 110$ m yr^{-1}; $\sigma_\omega = 26.5$.

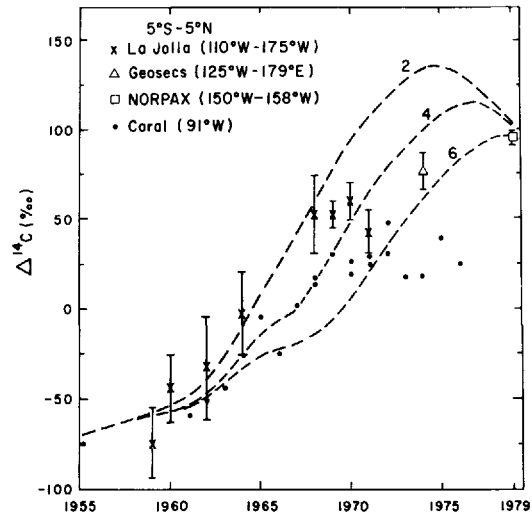

Figure 16. A comparison of the model calculated and measured time history of equatorial (5S–4N) mixed layer ^{14}C levels. Surface $\Delta^{14}C$ measurements include those made at La Jolla (Linick, 1978) during GEOSECS (Ostlünd and Stuiver, 1980), during Leg 3 of the FGGE shuttle and on corals collected on one of the Galapagos Islands (Druffel, 1980). Model calculated mixed layer ^{14}C time histories (---) are presented for three estimates of the exchange time (years) between subtropical surface water and the equatorial ocean. $W = 110$ m yr^{-1}; $\sigma_\omega = 26.5$.

poleward boundaries of the equatorial ocean. A net equatorward velocity of 1.4 ± 0.3 cm s^{-1} between 30° and 8° results in a transit time of 4–6 years. This meridional velocity agrees with the value of 1.2 cm s^{-1} calculated from the measured time change in subtropical mixed layer tritium concentrations (Michel and Suess, 1975). Also the above calculated equatorward velocity of 1.4 cm s^{-1} is nearly equal to the average geostrophic velocity of 1.3 cm s^{-1} (below the base of the mixed layer) calculated by Wyrtki (1981) at 5N and 5S. The agreement of these three independent calculations of meridional velocities supports the exchange time calculations of the equatorial mixing model and underscores the importance of meridional transport in the equatorial ocean. This 4–6 year exchange time implies a rapid transfer of dissolved chemical species between the subtropical and equatorial surface oceans. For example, recycling of fossil fuel derived CO_2 gas between the atmosphere and surface ocean can result from CO_2 gas invading into the subtropical surface water and subsequently evading from the equatorial mixed layer. Our model calculations suggest this recycling is occurring over the time scale of the anthropogenic atmospheric CO_2 input.

For the eastern equatorial Pacific, the lower mixed layer ^{14}C levels and the negligible change since 1970 (see Fig. 16) probably reflect the reduced exchange with water of subtropical characteristics which are located much further away from the equator in the EEP (Tsuchiya, 1968).

The results of this investigation indicate that the chemical properties of the central equatorial Pacific are dominated by meridional exchange with the water masses at the poleward boundaries of the equatorial ocean. The dominant transport process is geostrophic flow, resulting in an equatorial-wide upwelling transport rate of 47 Sv. This upwelling water is predominantly derived from depths shallower than 225 m ($\sigma_0 <$ 26.5). The likely origin of the water upwelling in the equatorial ocean is subtropical surface water which is exchanging with the equatorial ocean on a 4–6 year time scale.

Acknowledgments. We thank Harry Bryden, Steve Emerson and Taro Takahashi for their helpful comments. We would like to thank the crew of the R/V *Gyre*, Ed Slater (PCODF) and the members of the Quaternary Isotope Lab for their contributions in accomplishing the ^{14}C measurements. We are grateful to Leila Thompson for typing the manuscript and Floyd Bardsley for drafting the figures. This research was supported by Department of Energy Grant DE-AM06-76RL02225.

REFERENCES

Bevington, P. R. 1969. Data Reduction and Error Analysis for the Physical Sciences. McGraw Hill, N.Y., 336 pp.

Broecker, W. S. and T. H. Peng. 1974. Gas exchange rates between air and sea. Tellus, *26,* 21–35.

Broecker, W. S., T. H. Peng and M. Stuiver. 1978. An estimate of the upwelling rate in the equatorial Atlantic based on the distribution of bomb radiocarbon. J. Geophys. Res., *83,* 6179–6186.

Broecker, W. S., T. H. Peng and T. Takahashi. 1980. A strategy for the use of bomb-produced radiocarbon as a tracer for the transport of fossil-fuel CO_2 into the deep-sea source regions. Earth Planet. Sci. Letters, *49,* 463–468.

Broecker, W. S., T. Takahashi, P. Quay, D. Bos, D. Chipman and M. Stuiver. 1983. Carbon dioxide and radiocarbon budgets for the equatorial Pacific Ocean and the equatorial upwelling rate. J. Geophys. Res., (in press).

Crawford, W. and T. R. Osborn. 1981. Control of equatorial ocean currents by turbulent dissipation. Science, *212,* 539–540.

Druffel, E. 1980. Radiocarbon in annual coral rings of the Pacific and Atlantic Oceans. Ph.D. thesis, U.C.S.D. 213 pp.

Fine, R. A., W. H. Peterson, C. G. H. Rooth and H. G. Ostlünd. 1983. Cross equatorial tracer transport in the upper waters of the Pacific Ocean. J. Geophys. Res., *88,* 763–769.

Fine, R. A., J. L. Reid and H. G. Ostlünd. 1981. Circulation of tritium in the Pacific Ocean. J. Phys. Oceanogr., *11,* 3–14.

Fonselius, S. and H. G. Ostlünd. 1959. Natural radiocarbon measurements on surface water from the north Atlantic and the Arctic Sea. Tellus, *11,* 77–82.

Halpern, D. 1980. Vertical motion at the equator in the eastern Pacific (abstract). EOS., *61,* 998.

Kullenberg, G. 1974. An experimental and theoretical investigation of the turbulent diffusion in the upper layer of the sea. Inst. Phys. Oceanogr. Univ. Copenhagen Rep., *25,* 212 pp.

Linick, T. W. 1978. LaJolla measurements of radiocarbon in the oceans. Radiocarbon, *20,* 333–359.

McCreary, J. P. 1981. A linear stratified ocean model of the equatorial undercurrent. Phil. Trans. Roy. Soc. London, *298,* 603–635.

Michel, R. L. and H. E. Suess. 1975. Bomb tritium in the Pacific Ocean. J. Geophys. Res., *80,* 4139–4152.

Nydal, R., K. Lovseth and F. H. Skogseth. 1980. Transfer of bomb ^{14}C to the ocean surface. Radiocarbon, *22,* 626–635.

Osborn, T. R. 1980. Estimates of the local rate of vertical diffusion from dissipation measurements. J. Phys. Oceanogr., *10,* 83–89.

Ostlünd, H. G. 1981. NORPAX tritium results 1977–1980. Data Release #81-21. Tritium Laboratory, Rosensteil School of Marine and Atmospheric Science, University of Miami.

Ostlünd, H. G. and M. Stuiver. 1980. GEOSECS Pacific radiocarbon. Radiocarbon, *22,* 25–53.

Peng, T. H., W. S. Broecker, G. G. Mathieu and Y. H. Li. 1979. Radon evasion rates in the Atlantic and Pacific oceans as determined during the GEOSECS program. J. Geophys. Res., *84,* 2471–2786.

Reid, J. L. 1969. Sea-surface temperature, salinity and density of the Pacific ocean in summer and winter. Deep-Sea Res., *16* (Suppl.), 215–224.

—— 1973. The shallow salinity minima of the Pacific Ocean. Deep-Sea Res., *20,* 51–68.

Stuiver, M. 1980. ^{14}C distribution in the Atlantic Ocean. J. Geophys. Res., *85,* 2711–2718.

Stuiver, M. and H. A. Polach. 1977. Discussion: reporting of ^{14}C data. Radiocarbon, *19,* 253–258.

Stuiver, M. and S. W. Robinson. 1974. University of Washington GEOSECS North Atlantic ^{14}C results. Earth & Planet. Sci. Lett., *23,* 87–90.

Sverdrup, H. U., M. W. Johnson and R. H. Fleming. 1942. The Oceans. Prentice-Hall, N.J.

Takahashi, T. 1961. Carbon dioxide in the atmosphere and in the Atlantic Ocean water. J. Geophys. Res., *66,* 477–494.

Tsuchiya, M. 1968. Upper waters of the intertropical Pacific. Johns Hopkins Oceanogr. Stud., *4,* 50 pp.

Wyrtki, K. 1981. An estimate of equatorial upwelling in the Pacific. J. Phys. Oceanogr., *11,* 1205–1214.

Wyrtki, K., E. Firing, D. Halpern, R. Knox, G. J. McNally, W. C. Patzert, E. D. Stroup, B. A. Taft and R. Williams. 1980. The Hawaii to Tahiti shuttle experiment. Science, *211,* 22–28.

Received: *10 December, 1982;* revised: *26 April, 1983.*